Low-Temperature Kinetics of the Reaction of the OH Radical with Hydrogen Peroxide†

Andrei B. Vakhtin,‡ David C. McCabe,§ A. R. Ravishankara,§ and Stephen R. Leone*,||

JILA, National Institute of Standards and Technology and University of Colorado, Boulder, Colorado 80309, NOAA Aeronomy Laboratory, 325 Broadway R/AL2, Boulder, Colorado 80305, and Department of Chemistry and Biochemistry and CIRES, University of Colorado, Boulder, Colorado 80309

Received: April 10, 2003; In Final Form: September 30, 2003

The kinetics of the reaction of the OH radical with hydrogen peroxide, H_2O_2, are studied over a temperature range of 96−296 K. The low-temperature environment is provided by a pulsed Laval nozzle supersonic expansion of nitrogen with admixed H_2O_2. Hydrogen peroxide serves as both the OH radical photolytic precursor ($\lambda = 248$ nm) and a reactant. Laser-induced fluorescence of the OH radicals excited in the (1,0) band of the $A^2\Sigma^+ - X^2\Pi_i$ transition is used to monitor the kinetics of OH removal. The rate coefficient of the OH + H_2O_2 reaction (k_1) shows a negative temperature dependence within this temperature range, which can be expressed as $k_1 = (6.8 \pm 1.0) \times 10^{-13} \exp[(285 \pm 27)/T]$ cm^3 molecule^{-1} s^{-1}. The combined low- and high-temperature (literature) kinetic data form a U-shaped Arrhenius plot, which suggests that the reaction mechanism changes from direct abstraction (at high temperatures) to a mechanism involving formation of a hydrogen-bonded complex (at low temperatures). Atmospheric implications of the new low-temperature kinetic data are discussed.

Introduction

Hydrogen peroxide, H_2O_2, is formed in the atmosphere primarily via the reaction of two HO_2 radicals, thus converting two reactive HO_X (defined as the sum of OH and HO_2) radicals to an inactive form. Once formed, H_2O_2 is removed from the atmosphere via a variety of processes such as rainout, uptake onto condensed matter where it acts as an oxidant (e.g., oxidizing SO_2 to H_2SO_4), solar UV photolysis, and reaction with atmospheric free radicals. In the mid- to lower-troposphere, removal via rainout and uptake are the dominant loss processes for H_2O_2. However, in the upper troposphere and the stratosphere, the reaction of H_2O_2 with OH

$$OH + H_2O_2 \xrightarrow{k_1} HO_2 + H_2O \qquad (R1)$$

and photolysis of H_2O_2 to yield two OH radicals become the dominant loss processes for H_2O_2.

Formation of H_2O_2 and subsequent photolysis do not lead to a net loss of HO_X radicals. However, H_2O_2 formation followed by reaction R1 leads to the loss of two HO_X radicals. Since HO_X radicals play key roles in ozone formation in the upper troposphere and catalytic ozone destruction in the lower stratosphere, it is important to quantify any process, such as reaction R1, that significantly affects HO_X concentration. Therefore, the rate coefficients for reaction R1 at the temperatures of the upper troposphere and the lower stratosphere ($T = 190-250$ K) are needed.

While the rate coefficient for reaction R1 has been measured previously,[1−11] these measurements have been restricted to temperatures above 240 K because of the very small vapor pressure of H_2O_2 at low temperatures. As a consequence, k_1 has not been measured at the temperatures at which the reaction is most important in the atmosphere.

Furthermore, it is not clear whether extrapolation of the higher temperature data for k_1 to the 190−250 K temperature range is valid. Previous studies of the kinetics of reaction R1 show some divergence in the measured values of k_1 below room temperature. Reaction R1 exhibits a small activation energy ($E_a/R = 160$ K from 300 to 400 K[12]) although the kinetic isotope effect is large (e.g., k_1 is ≈3 times larger than the rate coefficient for the reaction of OH with D_2O_2 at 298 K[7]), suggesting a complex reaction pathway.

Hippler et al.[10,11] studied this reaction in shock tubes at temperatures up to 1680 K. They found that the reaction rate coefficient dramatically increases with temperature at $T > 900$ K. This behavior is indicative of a change in the reaction mechanism, probably from a mechanism involving complex formation at low temperatures to direct hydrogen abstraction at high temperatures.

Curved Arrhenius plots have been observed in studies of various reactions that involve the OH radical,[13−15] indicating that the OH radical readily forms hydrogen-bonded complexes with many H- and O-containing molecules.[15] Recently Brown et al.[14] reported that the rate coefficient for the reaction of OD with DNO_3 forms a U-shaped Arrhenius plot. They also reported that the rate coefficients of the OD + HNO_3 and OH + HNO_3 reactions show weak sigmoidal pressure dependence, particularly below room temperature. To explain the observed kinetic behavior, Brown et al. successfully applied a simple kinetic model that incorporates a reaction mechanism involving the formation of an intermediate cyclic six-membered ring hydrogen-bonded complex.[14] It is reasonable to expect that the OH + H_2O_2 reaction may proceed through a similar cyclic complex.

* Corresponding author. E-mail: srl@cchem.berkeley.edu.
† Part of the special issue "Charles S. Parmenter Festschrift".
‡ JILA. Present address: Southwest Sciences, Inc., Santa Fe, NM 87505.
§ NOAA and Department of Chemistry and Biochemistry and CIRES, University of Colorado.
|| JILA and Department of Chemistry and Biochemistry, University of Colorado. Present address: Departments of Chemistry and Physics and Lawrence Berkeley National Laboratory, University of California, Berkeley, CA 94720.

10.1021/jp030424q CCC: $25.00
Published on Web 11/11/2003

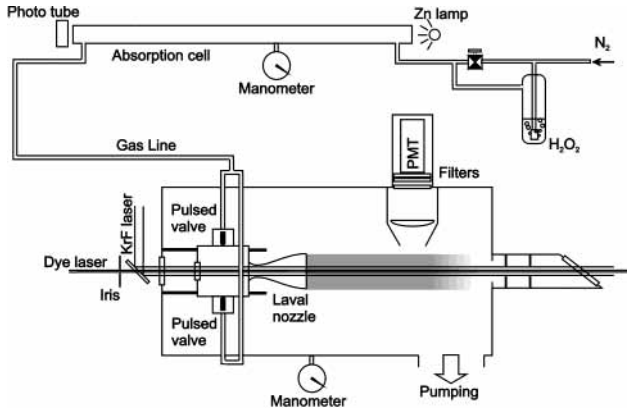

Figure 1. Schematic diagram of the experimental apparatus used to measure k_1.

Indeed, quantum chemical calculations predict that OH does form a five-membered ring complex with H_2O_2, bound by 17.1 kJ/mol (4.1 kcal/mol).[16] If such a complex is formed in reaction R1, one would expect a significant deviation of k_1 from Arrhenius behavior at lower temperatures.

For these reasons, it is important to measure the rate coefficient for reaction R1 at low temperatures. However, as mentioned earlier, conventional kinetic methods cannot be used because the saturation vapor pressure of H_2O_2 is too low at these temperatures. The Laval nozzle technique, however, is appropriate to measure k_1 at low temperatures.

In this work, we use a pulsed Laval nozzle apparatus[17−19] combined with pulsed photolysis and laser-induced fluorescence (LIF) of the OH radical to measure low-temperature rate coefficients for reaction R1 over the temperature range of 96−165 K. The rate coefficient was also measured at 296 K, using pulsed photolysis and LIF with a slow-flow system. The reaction rate coefficient shows a strong negative temperature dependence, which suggests that a complex-formation mechanism dominates at low temperatures.

Smith and co-workers have used the rate coefficient for the removal of a vibrationally excited radical by another species as a probe of the high-pressure limit (k_∞) for the association of the radical and the second species.[15,20] An unusually large rate coefficient of relaxation of a high-frequency vibration of the radical may indicate that the energy transfer occurs via a transient complex. In this work, we have also measured the rate coefficient for the removal of OH ($v = 1$) by H_2O_2

$$\mathrm{OH}\ (v = 1) + \mathrm{H_2O_2} \xrightarrow{k_2} \text{loss of OH}\ (v = 1) \qquad \text{(R2)}$$

at 296 K to further investigate the mechanism of reaction R1.

Experimental Section

The apparatus used in this work has been described previously.[17−19] Therefore, only a brief description will be given here. A schematic of the experimental setup is shown in Figure 1. The low-temperature environment is created by supersonic expansion of gas through a pulsed Laval nozzle, mounted in a nozzle block inside a stainless steel reaction chamber. Two pulsed solenoid valves supply an ≈5 ms gas pulse (nitrogen with admixed hydrogen peroxide) to a pre-expansion chamber in the nozzle block. The gas expands from the pre-expansion chamber through the Laval nozzle into the reaction chamber, which is pumped by a mechanical pump (60 L/s). A variable gate valve is used to limit the pumping speed in order to optimize the background pressure in the reaction chamber to appropriately collimate the supersonic flow. The background pressure is measured by a capacitance manometer.

The expansion through the Laval nozzle results in a collimated supersonic gas flow, which is characterized by a uniform Mach number, gas number density, and temperature along the flow axis for ≈20 cm.[17−19] The expansion conditions are characterized by using the Pitot tube method,[17,18] measuring the rotational temperature of the OH radicals from their LIF excitation spectra,[18] and directly measuring the flow velocity.[19] In this work, three different Laval nozzles are used to create supersonic flows of different temperatures: 96 ± 4 K, 110 ± 7 K, and 165 ± 14 K.[19]

The reaction and pre-expansion chambers have quartz windows, enabling introduction of laser beams along the axis of the gas flow to generate radicals photolytically (using an excimer laser) and for laser-based diagnostic techniques (using a frequency-doubled tunable dye laser) within the cooled expansion. In this work, LIF of OH is used as a probe. The laser beams exit the reaction chamber through an arm containing light baffles and a quartz Brewster-angle window, minimizing scattered light.

The OH radicals are produced by pulsed photolysis of H_2O_2 at 248 nm with the unfocused beam of a KrF excimer laser (≈30 mJ/pulse at a repetition rate of 10 Hz, fluence ≈8 mJ/cm^2). The frequency-doubled output radiation of a pulsed dye laser pumped by the second harmonic of a Nd:YAG laser is used for excitation of OH on the $Q_1(1)$ line of the (1,0) band of the $A^2\Sigma^+ \leftarrow X^2\Pi_i$ transition. LIF from OH is detected in the (1,1) and (0,0) bands of the $A \rightarrow X$ transition by a photomultiplier tube (PMT) equipped with a UV-band-pass filter and a narrow-band interference filter (310 ± 10 nm). The PMT, mounted 15 cm downstream of the Laval nozzle, detects the light through a quartz lens (5-cm diameter, 5-cm focal length). The lens focuses fluorescence from an ≈2 cm segment of the irradiated zone onto the PMT photocathode. The optics are appropriately shielded to minimize the effect of scattered light.

Temporal profiles of OH are recorded by monitoring the LIF intensity versus the delay between the photolysis and probe laser pulses. Typically, the signal from the photomultiplier is integrated over a 200-ns gate after a delay of 200 ns with respect to the probe laser pulse by a gated integrator. Active background subtraction is performed as described previously.[19] Normally, 20−100 experimental runs were averaged to obtain one OH temporal profile. The triggering of all units and devices is provided by a four-channel digital delay/pulse generator. Both the gated integrator and the pulse generator are interfaced to a computer, which is used to control the experiment and acquire data.

Nitrogen (99.999%), used as supplied from the cylinder, flows through a stainless steel line and a calibrated mass flow controller. An adjustable fraction of the N_2 flow is bubbled through a concentrated aqueous solution of hydrogen peroxide (>95 weight %, measured by titration with potassium permanganate) and then mixed into the main flow of the carrier gas. Downstream of the bubbler, all the tubing supplying the N_2/H_2O_2 mixture is made of PFA fluoropolymer. The concentration of hydrogen peroxide in the flow is determined by measuring the absorbance at 213.9 nm (Zn lamp, $\sigma_{213.9\mathrm{nm}}(H_2O_2) = 3.2 \times 10^{-19}$ cm^2 [12,21]) through a 100-cm absorption cell (see Figure 1). The total gas number density in the collimated supersonic flow is measured using the Pitot tube method, as described elsewhere.[18,19] The gas number density of H_2O_2 in the supersonic collimated flow is calculated from the total number density in the flow and the mole fraction of H_2O_2 in the gas mixture,

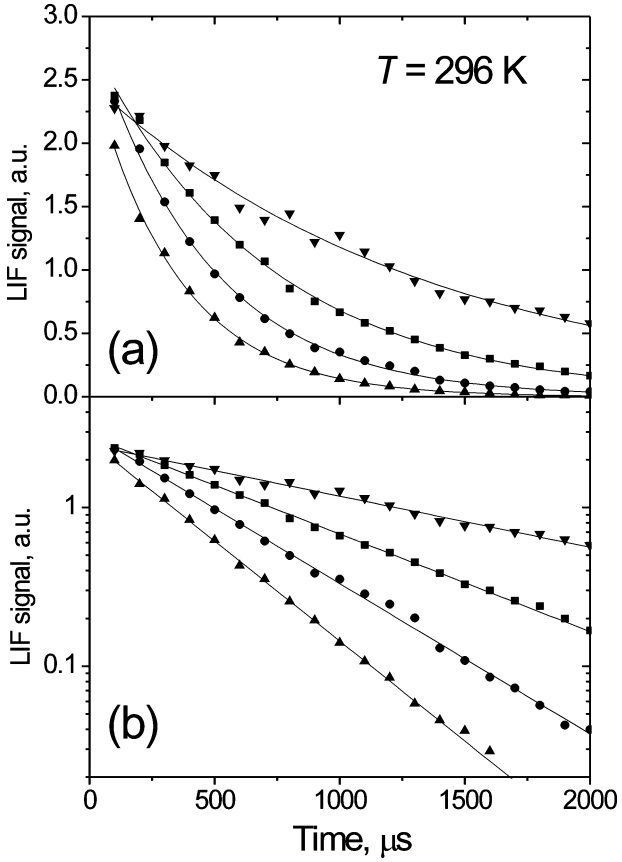

Figure 2. Examples of the OH decay profiles obtained at room temperature at different concentrations of H_2O_2, plotted in normal (a) and semilogarithmic (b) coordinates: ▼ $[H_2O_2] = 9.1 \times 10^{13}$ molecules cm^{-3}; ■ $[H_2O_2] = 4.5 \times 10^{14}$ molecules cm^{-3}; ● $[H_2O_2] = 8.6 \times 10^{14}$ molecules cm^{-3}; ▲ $[H_2O_2] = 1.3 \times 10^{15}$ molecules cm^{-3}. Lines show the fits to the single-exponential function (1).

obtained from the absorption measurements. The room-temperature value of k_1 is obtained in an identical manner, using the same apparatus, except that the N_2/H_2O_2 mixture continuously flows directly into the reaction chamber, bypassing the Laval nozzle.

The rate coefficient for reaction R2 was measured in a slow-flow system at 296 K using pulsed photolysis to produce OH ($v = 1$) and LIF to detect it, as described in detail elsewhere.[22] Briefly, H_2O_2 is photolyzed with 248-nm laser radiation; a small fraction (on the order of 1%) of the OH produced by photolysis of H_2O_2 at this wavelength is produced in the ($v = 1$) state. OH temporal profiles are measured using LIF: the $Q_1(1)$ line of the (0, 1) band of the OH ($A \leftarrow X$) electronic transition (≈346 nm) is excited by the probe laser; fluorescence in the (0, 0) band of the same electronic transition is detected by a PMT, mounted orthogonally to the photolysis and probe lasers and shielded with a band-pass filter to reject scattered laser light.

Results and Discussion

First, the room-temperature rate coefficient of reaction R1 was measured. Figure 2 shows examples of OH temporal profiles obtained at different concentrations of H_2O_2. Since the concentration of H_2O_2 was significantly larger (by a factor of at least 100) than the initial concentration of OH, the kinetics are pseudo-first-order in OH concentration. All measured temporal profiles could be fitted reasonably well to a single-exponential function. Figure 3 shows the first-order rate coefficient for OH loss (i.e., k') plotted versus the H_2O_2 concentration. From the slope of the straight line that fits the experimental data, the room-temperature rate coefficient is obtained as $k_1(296\ K) = (1.78 \pm 0.19) \times 10^{-12}$ cm^3 $molecule^{-1}$ s^{-1}, where the quoted uncertainty represents $2\sigma_c$ (σ_c is the "combined standard uncertainty," see below). This value is in good agreement with most available literature data,[2−9] and the current recommendations, $k_1(298\ K) = 1.7 \times 10^{-12}$ cm^3 $molecule^{-1}$ s^{-1}.[12,21]

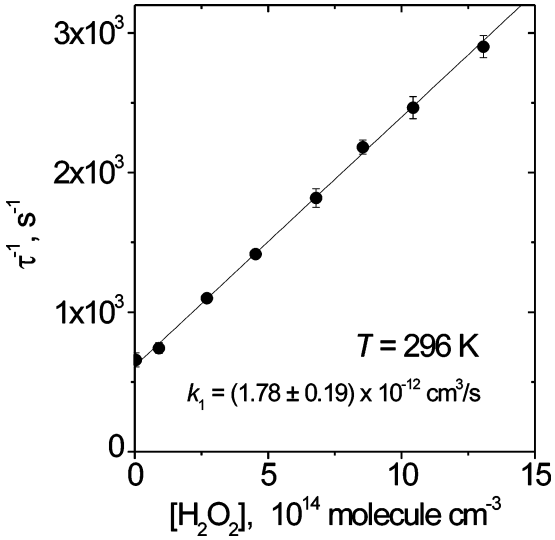

Figure 3. First-order OH loss rate coefficients versus concentration of H_2O_2 obtained at room temperature. For each concentration, the error bar indicates two standard deviations of the fit of the corresponding experimental OH decay profile by the single-exponential function. The line shows the $1/\sigma^2$-weighted linear least-squares fit.

At 296 K, the OH temporal profiles were recorded over several milliseconds (see Figure 2) in order to observe the decay of the OH signal over about 2 orders of magnitude, since the inverse decay time (k') is limited by the absolute value of k_1 and the H_2O_2 saturation vapor pressure.[23] While using the Laval nozzle expansion, the time window available for kinetic measurements is limited to about 200 μs by the length of the uniform collimated supersonic flow and the flow velocity.[18,19] Therefore, even with the highest attainable concentrations of H_2O_2 (limited by its saturation vapor pressure at the temperature of the laboratory and the throughput of the solenoid valves) in the Laval nozzle flow, we would not expect to be able to observe the decay of the OH signal over as large a dynamic range. As expected, in the low-temperature experiments, even with the highest obtainable H_2O_2 concentrations, we could detect only the initial parts of the OH temporal profiles. Figure 4a shows examples of OH temporal profiles obtained at "low" (1.7×10^{12} molecules cm^{-3}) and "high" (2.2×10^{14} molecules cm^{-3}) concentrations of hydrogen peroxide at $T = 110$ K. It is seen from Figure 4a that the "tail" ($t > 30$ μs) of the OH trace obtained at "high" $[H_2O_2]$ decays more steeply than that of the trace obtained at "low" $[H_2O_2]$. Although the difference is not large, it is consistent and reproducible. In numerous low-temperature experiments performed at different concentrations of H_2O_2, we always observed that the decay was steeper at higher $[H_2O_2]$. The rise during the first 10−30 μs could be due to rotational relaxation of OH.[24,25] The ripples in the OH decay profiles are mostly due to the inhomogeneity of the collimated flow;[18] they are reproducible and cannot be avoided.

To reduce the contribution of these ripples and of radial diffusion to the OH temporal profiles, we normalized the primary OH temporal profiles in each set of experiments by dividing them by a reference OH temporal profile, usually the

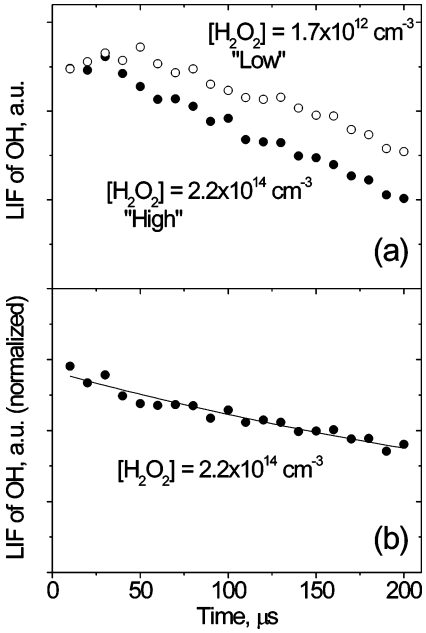

Figure 4. (a) Examples of the OH decay profiles obtained in Laval nozzle expansion at $T = 110$ K with "high" (●) and "low" (○) concentrations of H_2O_2. (b) Normalized OH profile, i.e., the ratio of the OH decay profiles obtained at "high" [H_2O_2] and "low" [H_2O_2] (●) and the single-exponential fit (line).

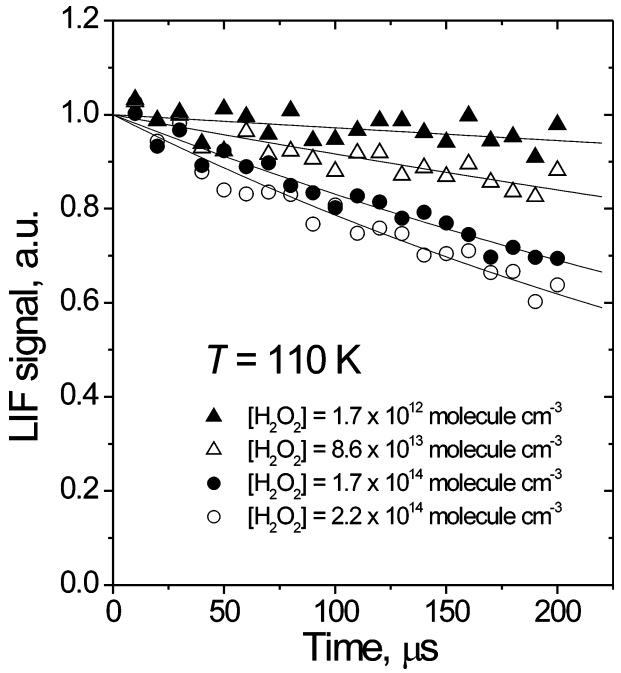

Figure 5. Normalized OH decay profiles obtained in Laval nozzle expansion at $T = 110$ K with different concentrations of H_2O_2. The profiles are scaled to coincide at zero time. Lines show the single-exponential fits to the experimental data.

one acquired with the smallest H_2O_2 concentration. This procedure has been described and justified by Orkin et al.[26] Figure 4b shows the normalized "high" H_2O_2 trace from Figure 4a (i.e., the ratio of the two traces shown in Figure 4a). Figure 5 presents examples of normalized OH decay profiles obtained at different concentrations of H_2O_2 at $T = 110$ K. The lines show the fits of the normalized decay profiles by the single-exponential function

$$S(t) = S_0 \exp(-t/\tau) \qquad (1)$$

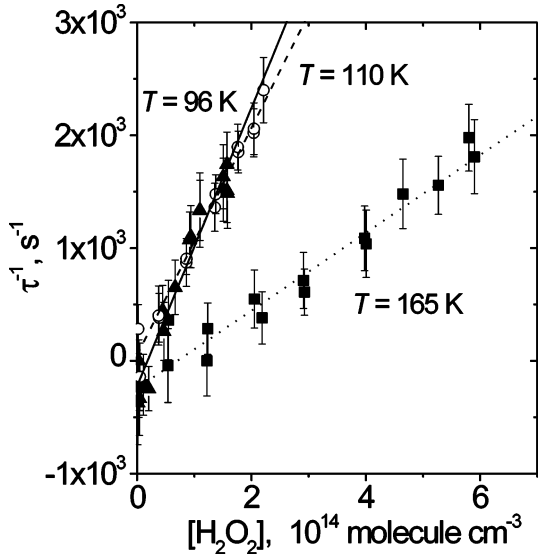

Figure 6. Pseudo-first-order plots for the OH + H_2O_2 reaction obtained at $T = 96$ K (▲), 110 K (○), and 165 K (■). The error bars indicate two standard deviations of the fits of the corresponding normalized experimental OH decay profiles by the single-exponential function (1). The lines show the $1/\sigma^2$-weighted linear fits for $T = 96$ K (solid line), 110 K (dashed line), and 165 K (dotted line).

TABLE 1: The Rate Coefficients of the OH + H_2O_2 Reaction (k_1) Measured at Different Temperatures; Buffer Gas N_2

T, K	total gas density, 10^{16} molecules cm^{-3}	[H_2O_2], 10^{12} molecule cm^{-3}	k_1,[a] 10^{-12} cm^3 molecule^{-1} s^{-1}
96 ± 4	1.9 ± 0.2	1.2−160	12.3 ± 4.5
110 ± 7	2.65 ± 0.45	1.7−220	10.1 ± 2.8
165 ± 14	3.5 ± 0.7	9.8−590	3.4 ± 1.4
296 ± 2	9.9 ± 0.1	3.4−1300	1.78 ± 0.19

[a] The indicated uncertainties represent $2\sigma_c$, where σ_c is a "combined standard uncertainty" that includes both statistical and systematic errors.

where S_0 and τ are the fitting parameters. It is assumed that the OH decays exponentially in the presence of H_2O_2 at low temperatures because pseudo-first-order conditions exist for OH. This assumption could not be directly verified at low temperatures by obtaining a full OH temporal profile (reduction of the OH signal by 2−3 orders of magnitude) with the present Laval nozzle apparatus. We compared the fit of the full normalized temporal profiles and truncated normalized temporal profiles, which had the first three points removed, to eq 1 in order to check for possible influence of the rise in the first part of the temporal profiles (see Figure 4a) upon the obtained values of k'. We observed no significant difference and used the fits to the full temporal profiles.

Figure 6 is a plot for three different temperatures of the first-order OH loss rate coefficients (k'), obtained by fitting the normalized experimental OH temporal profiles to eq 1, versus H_2O_2 concentration. The rate coefficients, obtained from the slopes of the linear fits of the experimental data in Figure 6, are presented in Table 1 along with the conditions under which the rate coefficients were obtained. The reported uncertainties of the measured rate coefficients represent $2\sigma_c$, where σ_c is the "combined standard uncertainty", which incorporates both statistical errors and the systematic errors. The values of σ_c were calculated according to NIST recommendations,[27] as described elsewhere.[18,19] For the room-temperature rate coefficient the main contributions to σ_c are the statistical scatter of the data and the uncertainty in the absorption cross section of H_2O_2 at 213.9 nm (assumed to be 5%[7]). For the low-temperature rate

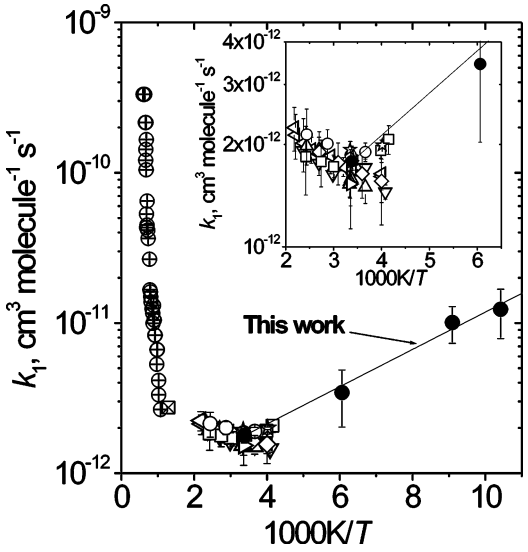

Figure 7. The rate coefficient of the OH + H_2O_2 reaction obtained in this work and taken from the literature, plotted in Arrhenius coordinates: (solid circle) this work; (box with crossed lines) Baldwin and Walker;[1] (triangle down) Keyser;[2] (triangle left) Sridharan et al.;[3] (triangle up) Wine et al.;[4] (tilted square) Kurylo et al.;[5] (open box) Lamb et al.;[6] (open circle) Vaghjiani et al.;[7] (open star) Lovejoy et al.;[8] (triangle right) Turnipseed et al.;[9] (crossed lines in circle) Hippler et al.[10,11] The line shows the fit of the data obtained in this work by the expression $k = A \exp(-T^*/T)$ (see text). The inset presents an expanded view of the data obtained within the temperature range of 165−500 K.

coefficients, σ_c is dominated by the uncertainty in the total gas number density in the Laval flow.[18,19]

Figure 7 is a plot of the rate coefficient k_1 measured in this work, together with the available literature data, as a function of $1/T$. At low temperatures k_1 shows a negative temperature dependence. The measured values of k_1, obtained in this work, can be described by the following expression:

$$k_1 = (6.8 \pm 1.0) \times 10^{-13} \exp[(285 \pm 27)/T] \quad \text{cm}^3 \text{ molecule}^{-1} \text{ s}^{-1}$$
$$T = 96-296 \text{ K} \qquad (2)$$

This expression is obtained by $1/\sigma^2$-weighted fitting of the experimental data to the formula $k = A \exp(-T^*/T)$ with the fitting parameters A and T^*. The uncertainties indicated for A and T^* represent two standard deviations. The result of the fit is shown in Figure 7 as a solid line. Although the fitting formula is formally identical to the Arrhenius expression, A and T^* should be considered purely empirical parameters valid only within the indicated temperature range, rather than physically meaningful quantities.

Within the full temperature range where experimental data are available, $96 < T < 1680$ K, the Arrhenius plot of the rate coefficient k_1 is U-shaped. As discussed by Hippler et al.,[11] the sharp change at around 900 K is probably due to the reaction mechanism changing from direct abstraction at high temperatures to the formation of an intermediate complex at lower temperatures. This is in accord with quantum-chemical calculations by Wang et al.[16] They used the CCSD(T)//B3LYP method to locate a hydrogen-bonded OH···H_2O_2 five-membered ring complex with a binding energy of 17.1 kJ mol^{-1} (4.1 kcal mol^{-1}). The complex-formation mechanism is also supported by the observations that, although reaction R1 at $T < 900$ K apparently proceeds with little or no activation barrier, the absolute value of k_1 is relatively low in this temperature range, and the kinetic isotope effect for the reaction is relatively strong (k_1 is ≈3 times larger than the rate coefficient for the reaction of OH with D_2O_2 at 298 K[7]).

The rate coefficient for the removal of OH ($v = 1$) by H_2O_2, k_2, is measured to be $(3.5 \pm 0.3) \times 10^{-11}$ cm^3 molecule^{-1} s^{-1} at 296 K. This rate coefficient includes an estimated correction of about 20% to account for the quenching of OH ($v = 1$) by H_2O, which is introduced into the flow, along with H_2O_2, when N_2 is bubbled through the H_2O_2/H_2O solution. With a 95 weight % H_2O_2 solution, the effluent from the bubbler contains H_2O_2 and H_2O in a mole ratio of about 2:1.[23] For the quenching of OH ($v = 1$) by H_2O, we use an average of several reported rate coefficients,[28−31] 1.4×10^{-11} cm^3 molecule^{-1} s^{-1}. This large rate coefficient may corroborate the formation of the OH···H_2O_2 complex.[15] However, loss of OH ($v = 1$) by resonant intermolecular energy transfer (i.e., without formation of the complex) cannot be ruled out, since OH and H_2O_2 are closely vibrationally resonant. For more definitive conclusions, measurements of the rate coefficient for removal of OD ($v = 1$) by H_2O_2, where intermolecular V−V energy exchange is much less important, are necessary. These measurements are now in progress.

Formation of an intermediate weakly bound complex, followed by competing dissociation of the complex back to the reactants and to the reaction products, may result in unusual temperature and pressure dependence of the overall reaction rate coefficient.[13−15] The particular kinetic behavior strongly depends on the barriers to the backward and forward dissociation of the complex and the structure and "rigidity" of the corresponding transition states. Quantum chemical calculations aimed at evaluating the height and the profile of the "exit" barrier (associated with dissociation of the complex into the reaction products HO_2 and H_2O) are underway at NOAA. Knowledge of these features of the potential energy surface will be helpful in evaluating a kinetic model for this reaction, similar to that successfully applied by Brown et al.[14] for the OH + HNO_3 reaction.

Given the dramatic non-Arrhenius behavior of reaction R1 over the temperature range shown in Figure 7, and the uncertainty of the rate coefficients reported here, we must note that the quality of the fit of our data to an Arrhenius expression (with negative activation energy) may be simply fortuitous. In other words, our data certainly do not prove that k_1 reaches its minimum near 296 K. Nevertheless, these data do show that k_1 begins increasing with decreasing temperature at some point. Some previous measurements of k_1, particularly the measurements of Lamb et al.,[6] do show an increase below room temperature; however, these measurements are not considered in current recommendations.[12,21] While it is possible that the rate coefficient continues decreasing below room temperature to ≈240 K or even lower, it is also possible that some previous measurements below room temperature[2−5] have underestimated k_1 due to loss of H_2O_2 to the walls of the reactor at low temperature.

For atmospheric purposes, direct measurements of k_1 between 190 and 240 K are needed. However, the Laval nozzle expansion method may not be successful at these temperatures, because of the limited time scale available to monitor the kinetics with this method. It will be particularly difficult to measure the rate coefficient accurately at 190−240 K, because it will be smaller at these temperatures than at the temperatures studied in this work.

Interpolation of expression 2 for k_1 to the temperature range 190−240 K can provide an estimate for k_1 in the absence of direct measurements of the rate coefficient at these temperatures.

At 200 K, expression 2 gives $k_1 = (2.8 \pm 0.9) \times 10^{-12}$ cm^3 molecule^{-1} s^{-1}, while extrapolation of the current JPL[12] and IUPAC[21] recommendation gives $k_1 = (1.3 \pm 0.6) \times 10^{-12}$ cm^3 molecule^{-1} s^{-1}. Clearly, extrapolation of the currently recommended value of k_1[12,21] to the lower temperatures of the atmosphere may result in a value of k_1 that is quite inaccurate. If k_1 is indeed higher than currently recommended, atmospheric models underestimate the loss of HO_X in the upper troposphere and lower stratosphere due to reaction R1. It is also noteworthy that expression 2 yields values of k_1 around 240−250 K that agree well with the value of k_1 at these temperatures reported by Lamb et al.[6] and Lovejoy et al.[8]

It is possible that the reaction of OH with H_2O_2 that we observe at low temperatures does not yield the products quoted for reaction R1; i.e., the reaction we observe is only producing an OH···H_2O_2 complex that is not in turn dissociating to form H_2O and HO_2. However, we do not believe that this is the case. The binding energy of the OH···H_2O_2 complex is predicted to be quite small, 17.1 kJ/mol,[16] so that the rate coefficient for formation of the OH···H_2O_2 complex, if that complex could only dissociate back to the reactants, would be quite small at the pressures of these experiments. Using the Troe method for barrierless association reactions[32,33] with the binding energy, structure, and vibrational frequencies of the OH···H_2O_2 complex reported by Wang et al.,[16] we estimated an upper limit for the termolecular rate coefficients for formation of the OH···H_2O_2 complex from reactants. The estimates show that, at the gas number densities used in the experiments (see Table 1), the bimolecular association rate coefficient would be at least 3 orders of magnitude smaller than the observed k_1 between 96 and 296 K. This is evidence that the reaction of OH with H_2O_2 that we are observing is producing HO_2 and H_2O. We attempted to experimentally verify that HO_2 is formed by reaction R1 at low temperatures by adding NO, which should react rapidly with HO_2 to form OH,[34] to the gas mixture flowing through the Laval nozzle. These attempts were not successful due to experimental problems and were not further pursued.

Since the supersonic expansion is greatly supersaturated with H_2O_2, formation of dimers and larger clusters of H_2O_2 could occur within the expansion. Also, H_2O_2 might form clusters with water introduced into the flow, along with H_2O_2, when nitrogen is bubbled through the H_2O_2/H_2O solution. The rate coefficients for the reactions of OH with the H_2O_2 dimers and clusters could be significantly different than k_1. However, formation of dimers and clusters should be slow at the pressures of these experiments. We again used the Troe method[32,33] and the binding energy, structure, and vibrational frequencies of the C_i dimer of H_2O_2 and the $H_2O_2-H_2O$ complex described by González et al.[35] to estimate upper limits for the rate coefficients for formation of those complexes. The estimates show that these two processes convert no more than 0.02% of H_2O_2 within the available time at the temperatures of this study; therefore they cannot affect the observed rate of OH decay.

In addition to direct studies of k_1 in the temperature range needed for atmospheric purposes, further elucidation of the mechanism of this reaction could be provided by an investigation of the primary and secondary H/D kinetic isotope effects on k_1 at low and high temperatures. Direct study of the products of reaction R1 at temperatures below 240 K would also be helpful.

Acknowledgment. The authors gratefully acknowledge the support of this research by the National Aeronautics and Space Administration (Grant NAG5-8923, NAG5-13339, and the Upper Atmosphere Research Program). D.C.M. acknowledges a National Science Foundation Graduate Research Fellowship. S.R.L. wishes to acknowledge the many profound interactions with Professor Charles Parmenter throughout his career.

References and Notes

(1) Baldwin, R. R.; Walker, R. W. *J. Chem. Soc., Faraday Trans. 1* **1979**, *75*, 140.
(2) Keyser, L. F. *J. Phys. Chem.* **1980**, *84*, 1659.
(3) Sridharan, U. C.; Reimann, B.; Kaufman, F. *J. Chem. Phys.* **1980**, *73*, 1286.
(4) Wine, P. H.; Semmes, D. S.; Ravishankara, A. R. *J. Chem. Phys.* **1981**, *75*, 4390.
(5) Kurylo, M. J.; Murphy, J. L.; Haller, G. S.; Cornett, K. D. *Int. J. Chem. Kinet.* **1982**, *14*, 1149.
(6) Lamb, J. J.; Molina, L. T.; Smith, C. A.; Molina, M. J. *J. Phys. Chem.* **1983**, *87*, 4467.
(7) Vaghjiani, G. L.; Ravishankara, A. R.; Cohen, N. *J. Phys. Chem.* **1989**, *93*, 7833.
(8) Lovejoy, E. R.; Murrels, T. P.; Ravishankara, A. R.; Howard, C. J. *J. Phys. Chem.* **1990**, *94*, 2386.
(9) Turnipseed, A. A.; Vaghjiani, G. L.; Gierczak, T.; Thompson, J. E.; Ravishankara, A. R. *J. Chem. Phys.* **1991**, *95*, 3244.
(10) Hippler, H.; Troe, J. *Chem. Phys. Lett.* **1992**, *92*, 333.
(11) Hippler, H.; Neunaber, H.; Troe, J. *J. Chem. Phys.* **1995**, *103*, 3510.
(12) Sander, S. P.; Friedl, R. R.; Golden, D. M.; Kurylo, M. J.; Huie, R. E.; Orkin, V. L.; Moortgat, G. K.; Ravishankara, A. R.; Kolb, C. E.; Molina, M. J.; Finlayson-Pitts, B. J. *Chemical Kinetics and Photochemical Data for Use in Atmospheric Studies, Evaluation 14*; JPL Publication No. 02-25; Jet Propulsion Laboratory: Pasadena, CA, 2003.
(13) Troe, J. *J. Chem. Soc., Faraday Trans.* **1994**, *90*, 2303.
(14) Brown, S. S.; Burkholder, J. B.; Talukdar, R. K.; Ravishankara, A. R. *J. Phys. Chem. A* **2001**, *105*, 1605.
(15) Smith, I. W. M.; Ravishankara, A. R. *J. Phys. Chem. A* **2002**, *106*, 4798.
(16) Wang, B.; Hou, H.; Gu, Y. *Chem. Phys. Lett.* **1999**, *309*, 274.
(17) Lee, S.; Hoobler, R. J.; Leone, S. R. *Rev. Sci. Instrum.* **2000**, *71*, 1816.
(18) Vakhtin, A. B.; Lee, S.; Heard, D. E.; Smith, I. W. M.; Leone, S. R. *J. Phys. Chem. A* **2001**, *105*, 7889.
(19) Vakhtin, A. B.; Murphy, J. E.; Leone, S. R. *J. Phys. Chem. A*, in press.
(20) Smith, I. W. M. *J. Chem. Soc., Faraday Trans.* **1997**, *93*, 3741.
(21) Atkinson, R.; Baulch, D. L.; Cox, R. A.; Hampson, R. F.; Kerr, J. A.; Rossi, M. J.; Troe, J. *J. Phys. Chem. Ref. Data* **1997**, *26*, 521.
(22) McCabe, D. C.; Brown, S. S.; Gilles, M. K.; Talukdar, R. K.; Smith, I. W. M.; Ravishankara, A. R. *J. Phys. Chem. A* **2003**, *107*, 7762.
(23) Scatchard, G.; Kavanagh, G. M.; Ticknor, L. B. *J. Am. Chem. Soc.* **1952**, *74*, 3715.
(24) Kliner, D. A. V.; Farrow, R. L. *J. Chem. Phys.* **1999**, *110*, 412.
(25) Sims, I. R.; Smith, I. W. M.; Bocherel, P.; Defrance, A.; Travers, D.; Rowe, B. R. *J. Chem. Soc., Faraday Trans.* **1994**, *90*, 1473.
(26) Orkin, V. L.; Huie, R. E.; Kurylo, M. J. *J. Phys. Chem.* **1996**, *100*, 8907.
(27) Taylor, B. N.; Kuyatt, C. E. *Guidelines for Evaluating and Expressing the Uncertainty of NIST Measurement Results*; NIST Technical Note 1297; US Government Printing Office: Washington, DC, 1994.
(28) Kneba, M.; Wolfrum, J. *Annu. Rev. Phys. Chem.* **1980**, *31*, 47.
(29) Smith, I. W. M.; Williams, M. D. *J. Chem. Soc., Faraday Trans. 2* **1985**, *81*, 1849.
(30) Raiche, G. A.; Jeffries, J. B.; Rensberger, K. J.; Crosley, D. R. *J. Chem. Phys.* **1990**, *92*, 7258.
(31) Silvente, E.; Richter, R. C.; Hynes, A. J. *J. Chem. Soc., Faraday Trans.* **1997**, *93*, 2821.
(32) Troe, J. *J. Chem. Phys.* **1977**, *66*, 4745.
(33) Troe, J. *J. Chem. Phys.* **1977**, *66*, 4758.
(34) Seeley, J. V.; Meads, R. F.; Elrod, M. J.; Molina, M. J. *J. Phys. Chem.* **1996**, *100*, 4026.
(35) Gonzalez, L.; Mo, O.; Yanez, M. *J. Comput. Chem.* **1997**, *18*, 1124.